Photonics and Nanostructures – Fundamentals and Applications 28 (2018) 56–60

Contents lists available at ScienceDirect

Photonics and Nanostructures – Fundamentals and Applications

journal homepage: www.elsevier.com/locate/photonics

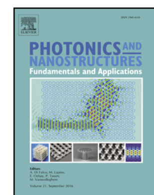

Invited Paper

Investigation of single-mode vertical-cavity surface-emitting lasers with graphene-bubble dielectric DBR

Baolu Guan [a,b,*], Pengtao Li [a], Shamsul Arafin [b], Yazeed Alaskar [b], Kang L. Wang [b]

[a] Key Laboratory of Opto-electronics Technology, Ministry of Education, Beijing University of Technology, Beijing 100124, China
[b] Device Research Laboratory, Department of Electrical Engineering, University of California at Los Angeles, CA 90095, USA

A R T I C L E I N F O

Article history:
Received 26 February 2017
Received in revised form 20 June 2017
Accepted 31 July 2017
Available online 4 August 2017

A B S T R A C T

An inter-cavty contact single mode 850 nm VCSEL was fabricated with a graphene assisted self-assembly curved dielectric bubble Bragg mirror for the first time. Taking the advantage of graphene's uniform low surface energy, the low cost dielectric bubble DBR (Si_3N_4/SiO_2) was deposited on top of the graphene/half-VCSEL structure via van der Waals Force (vdWF) without using any additional spacing elements and sacrificial layer release-etch process. The continuous-wave operating VCSELs with an aperture diameter of 7 μm exhibit single-mode output power of more than 1 mW with a slope efficiency of 0.2 W/A. The sidemode suppression ratios are >40 dB. This novel modification into the lasers can also be applied to a variety of other optoelectronic devices, such as resonance photodetecter and super narrow linewidth VCSEL.

© 2017 The Authors. Published by Elsevier B.V. This is an open access article under the CC BY-NC-ND license (http://creativecommons.org/licenses/by-nc-nd/4.0/).

1. Introduction

Single mode and high speed vertical-cavity surface-emitting lasers (VCSELs) are particularly promising for the development of functional integrated optics [1–3]. VCSELs with a single transverse mode are of great importance because they enable efficient coupling with fiber and prevent excessive pulse broadening over long transmission distances caused by chromatic dispersion in the fiber. VCSELs possess advantageous properties, such as circle beam shape, catastrophic optical damage (CCD)-free and two-dimensional integration [4–7], but they typically that will be more obvious in multiple transverse modes as a result of strong index confinement from the oxide layers [8]. Obtaining single mode operation from these VCSELs usually requires a reduced cavity cross-section area to decrease the number of transverse modes that are supported. However, this produces a reduced active volume, which can substantially limit the output power of the fundamental mode. Therefore, demonstrating high power fundamental mode emission from a VCSEL has to-date been a challenge. Controlling the transvers modes in VCSELs have already been performed by the technique of anti-resonant patterning [9], surface relief [10], tunnel junction patterning [11] and photonic crystals [12]. Unfortunately, these mode-control techniques in the device involve undesired high threshold current, complex process conditions and expensive technology.

Graphene, a monolayer of carbon atoms with a regular sp^2-bonded atomic-scale hexagonal pattern, exhibits high carrier mobility, massless Dirac fermions, mechanical strength, thermal conductivity and stable chemical characteristics [13–15]. Due to such extraordinary properties, graphene recently came to be used as a buffer layer, allowing crystalline growth of III–V compound semiconductor via van der Waals epitaxy (vdWE) [16,17]. In addition, some other applications realize multi-use of graphene as transparent conducting electrodes in flexible optoelectronic devices and also for the growth of vertical high-performance optical composites that require formation of initial films with high-Q optical function. Here, we studied the VCSELs with graphene as a transparent electrode and deposited buffer layer. Here, chemical vapor deposition (CVD)-graphene was transferred on a half-VCSEL structure as a transparent electrode. Then a dielectric Si_3N_4/SiO_2 distributed Bragg-reflector (DBR) was deposited via vdWF on graphene, taking the advantage of graphene's uniform low surface energy. Without using any additional spacing elements, the built-in strain gradient of Si_3N_4/SiO_2 results in a concave curvature of bubble DBR and allows an easy alignment with VCSELs center apertures. This bubble DBR has increased the higher order mode loss and the gain for the fundamental mode by confining the transvers optical field to the top DBR. Thanks to the three-dimensional model of curved mirror, it showed that the insert airgap section increased reflectivity and bandwidth. Comparing

* Corresponding author at: Key Laboratory of Opto-electronics Technology, Ministry of Education, Beijing University of Technology, Beijing 100124, China.
E-mail address: Gbl@bjut.edu.cn (B. Guan).

http://dx.doi.org/10.1016/j.photonics.2017.07.005
1569-4410/© 2017 The Authors. Published by Elsevier B.V. This is an open access article under the CC BY-NC-ND license (http://creativecommons.org/licenses/by-nc-nd/4.0/).

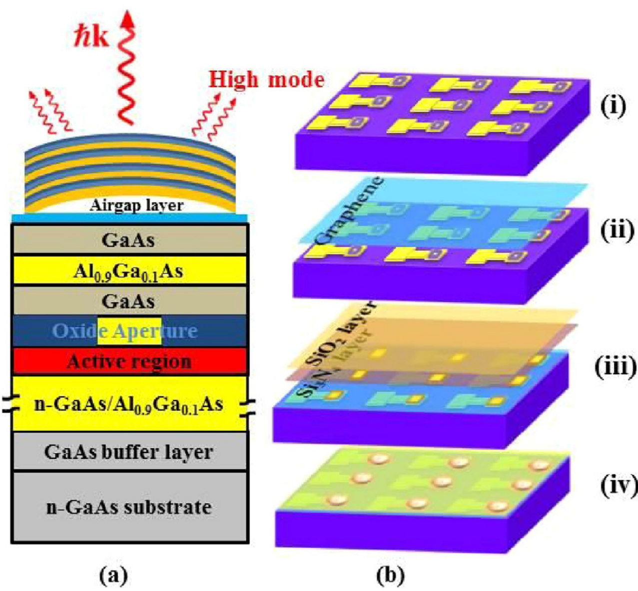

Fig. 1. (a) Schematic cross-sectional view of the top-emitting VCSEL structure, (b) process flow of VCSEL fabrication in this study, where CVD graphene films are transferred to a half-VCSEL with top p-metal contact. Finally, the dielectric Si_3N_4/SiO_2 layers were deposited on top of the graphene layer.

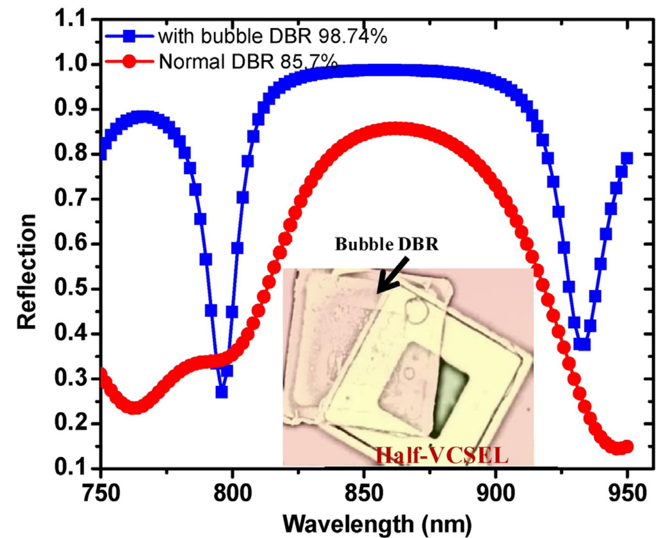

Fig. 2. Reflectivity spectra of the normal and bubble DBR, consisting of seven-pair of Si_3N_4/SiO_2 in VCSELs. A higher refractive index contrast due to the airgap at the dielectric/semiconductor interface helps to obtain a high reflectivity as well as wide stopband in the spectrum.

to the initial structure design without bubble DBR, the reflectivity and the bandwidth has been increased by ~15% and ~73%. The spectral characteristics of these VCSELs under continue wave (CW) show that the single mode output was more than 1 mW and the slope efficiencies of Gr-VCSEL is 0.2 W/A by less than 12 mA. In this study, we introduce the epitaxial graphene as an important platform to regrow high-quality dielectrics multilayers on 2D materials via vdWF. This device structure allows us to suppress higher-order modes in large-area VCSELs, resulting in high quality single-mode devices. At the same time, it reduces the contact resistance in the device, which should ultimately improve the excitation potentiality high-speed performance of VCSELs.

2. Fabrication and process

The scheme view of the VCSELs with integrated graphene is shown in Fig. 1(a). The half-VCSEL vertical structure is the same as that of conventional 850 nm VCSELs without top DBR [18]. The bottom mirror consists of a 30-period Si-doped $Al_{0.9}Ga_{0.1}As/Al_{0.12}Ga_{0.88}As$ DBR. The active region has three $Al_{0.3}Ga_{0.7}As/Al_{0.12}In_{0.18}Ga_{0.7}As$ quantum wells sandwiched in one-λ cavity. The p-mirror consists of a 2-period carbon-doped $Al_{0.9}Ga_{0.1}As/Al_{0.12}Ga_{0.88}As$ DBR. This part is often referred to as a "half-VCSEL". Lateral optical confinement is formed by applying a 60-nm-thick oxide layer of $Al_{0.98}Ga_{0.02}As$ to define gain and loss regions in the optical cavity. The second chip of the top bubble DBR consists of 7-pair dielectric Si_3N_4/SiO_2 layers formed on the graphene. The device fabrication procedure is schematically shown in Fig. 1(b). (i) "half-VCSEL" was fabricated by standard laser fabrication process; (ii) The graphene films were grown on copper foil using CVD. We used standard graphene transfer process where a thin layer of PMMA was coated on the top of graphene film [19] Followed by etching copper foil by Cu etchant, the graphene/PMMA film was transferred to half-VCSEL substrate. (iii) After optical lithography to pattern the graphene electrode layer by O_2 plasma, the 7-pair Si_3N_4/SiO_2 layers were deposited by plasma enhanced chemical vapor deposition (PECVD) and (iv) the bubbled DBR was formed due to built-in strain increasing. As key advantage of using 2D graphene layer gives us low transvers series resistances to significance allow high modulation speed Gr-VCSEL. Using CVD synthesis and the PMMA transfer method, the size of graphene conducting film can be easily scaled up which has no fundamental limit in VCSEL fabrication process.

3. Experiment and results

In order to demonstrate the effect of the dielectric bubble DBR on the device performance, the reflectivity spectrum is compared with the one without bubble DBR, as shown in Fig. 2. The stopwidth can be increased in the bubble DBR without any trade-off in the reflectivity spectrum. This allows a maximizing broadband width and reflectivity, which given the specific requirement on a minimal reflectivity that can be tolerated by laser emitting. The bandwidth and reflectivity can be increased by ~73% and 15%, respectively, in comparison to the initial DBR structure without bubble DBR. As a three dimensional model of bubble DBR shows that the induced airgap section causes a high index contrast between the interface of semiconductor/air and dielectric/air. Hence, the larger the contrast is, the wider the bandwidth [20]. Fig. 3 demonstrates this fact by regrow the same high reflectivity contours for a larger contrast index, fine-inserted airgap layer, and for seven-period Si_3N_4/SiO_2 bubble DBR. The SEM image in Fig. 3(a) shows that the transfer process of epitaxial graphene layer have been completely finished, including rectangular p-GaAs contact from the half-VCSEL surface. And the Raman spectrum in Fig. 3(b) indicates that the quality of the graphene is maintained during the transfer (very low disorder-induced "D" peak in the spectra). The large intensity ratio ($I_{2D}/I_G > 2$) of 2D band (~2688 cm^{-1}) over G band (~1592 cm^{-1}) is associated with monolayer graphene. In addition, the optimized process means that broadband design also automatically results in large fabrication tolerance on the thickness of airgap. Larger fabrication tolerance in high contrast dielectric bubble DBR was first experimentally demonstrated by our group in the context of VCSELs. In our method, the Si_3N_4/SiO_2 DBR on the graphene surface induces an accumulated internal built-in strain resulting a weak adhesion to graphene, as shown in Fig. 3(d). However, for obtaining perfect graphene and bubble DBR in laser device, it is critical to select a proper strained material that satisfy the following conditions for uniform with a high yield: first, there is no chemical reaction with Carbon and no solubility in Carbon (and vice versa) to obtain defect-

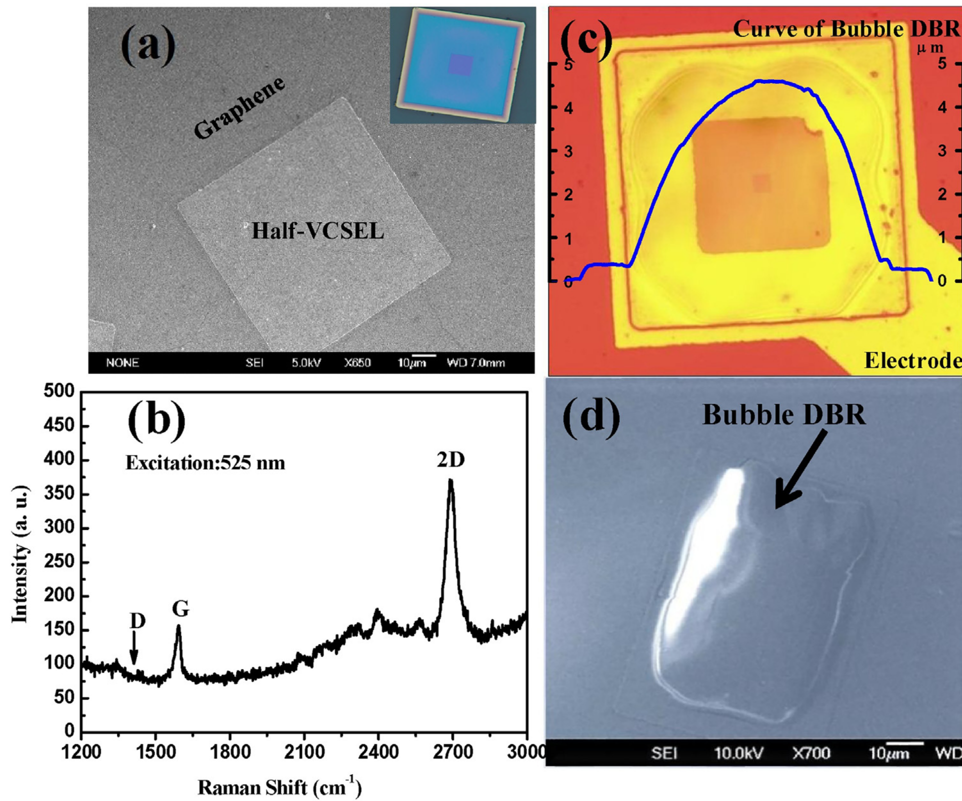

Fig. 3. (a) Plane-view SEM image of a half-VCSEL structure after Graphene was transferred onto it. (b) Representative Raman spectrum of the graphene, indicating single layer graphene and there is no damage during the transfer (no D peak). (c and d) Optical microscope and SEM images of the complete VCSEL with bubble dielectric DBR. A mechanical surface scan of the bubble DBR indicating a curvature of approximately 4.5 μm, as shown in inset of (c).

free graphene; second, the adhesion energy required for graphene is weaker than between graphene and p-GaAs; and there is enough high built-in strain energy to separate from the graphene/GaAs interface. The adhesion energies between graphene and these substrate materials can be expected as $\Gamma = 2(\gamma_{Gr} \times \gamma_{surface})^{1/2}$, where γ_{Gr} is the surface energy of graphene and $\gamma_{surface}$ is the surface energy of substrate material [21]. As reported, the values of adhesion energy derived from the measured monolayer grpahene/SiO_2 is $0.45 \pm Jm^{-2}$, however to the GaAs (110) surface, the energy is about $0.86 Jm^{-2}$, so the values of adhesion energy of monolayer graphene/GaAs is $\Gamma = 2(\gamma_{Gr} \times \gamma_{GaAs})^{1/2} = 0.829 Jm^{-2}$, which near more than two times of graphene/SiO_2 adhesion energy. In addition, the surface roughness also affects the adhesion between graphene and their substrates, making the adhesion energy of $(0.275–0.4) Jm^{-2}$ [22–24]. Thus the Si_3N_4/SiO_2 DBR finds an airgap on the graphene surface, and the DBR is inherently formed at the center of the oxide aperture. Airgap layer is important because it increases the electrical properties of the graphene (such as carrier mobility) as well as the ballistic nature of charge transport. Such selective and self-assembled dielectric layers with airgap via vdWF on graphene is reported for the first time, which will improve the optical and electric properties of the devices.

The electrical properties of CVD-grown graphene are measured. For that, graphene-based Hall-bar devices with evaporated Cr/Au contacts lying on SiO_2/Si substrate. A representative plot of the channel resistance (R) as a function of the voltage (V) measured from the Hall bars is shown in Fig. 4(a). The optical image of a representative device and band energy diagram are shown inset. In contrast to pristine graphene, the Si_3N_4/SiO_2 regrow onto the graphene is like typical graphene layers transferred on half-VCSEL substrate. I–V channel resistance calculated from the maximum channel resistance was 5 KΩ. Similarly, the Hall resistance R_{xx} measured from Hall-bar was in the range of 2145–2185 Ω, the mobility was in the range of 1000–2000 $cm^2V^{-1}s^{-1}$, depending on the carrier density (Fig. 4b). These mobility values are comparable to Hall mobility values measured from pristine graphene [25]. These electrical measurement results indicate that graphene maintains its quality even after the required device processing.

Fig. 5 shows the room-temperature light-current (*L–I*) characteristics, and voltage-current (*V–I*) characteristics of the fabricated VCSELs. The microscript image of Gr-VCSEL with dielectric bubble DBR is exhibited in inserts. The maximum light output power is 1.1 mW at an injection current of 20 mA for such devices, exhibiting higher slope efficiency. The slope efficiencies of the device is 0.2 W/A at less than 12 mA. The threshold current of 1.8 mA, which corresponds to threshold current density of only 2.6 kA/cm^2, is achieved with oxide aperture diameter of the device is 7 μm. This result suggests that no serious dislocations are introduced into the laser structure through the regrow process. But the light output power of the device can be further increased by optimizing the processing involved in the deposition of top bubble dielectric DBR. The maximum optical gain can be achieved by aligning the lasing wavelength with the Bragg wavelength of bubble DBR. This could be done by adjusting the strain of dielectric Si_3N_4/SiO_2 layers [26,27]. A higher driving voltages could be attributed to the high contact resistance at the metal/graphene/semiconductor interface, serving as a top ohmic contact of the device. Introducing an annealing thin metal contact layer is expected to reduce such contact resistance. The spectra of the devices at a bias of 20 mA are shown in inset of Fig. 5. This types of VCSELs exhibited single mode light output and the center wavelength of around 858.5 nm, exhibited single mode operation with side-mode suppression ratio of over 20 dB at RT. Results show that a built-in strain gradient resulted in a concave curvature of the top DBR and allows an easy and tilt

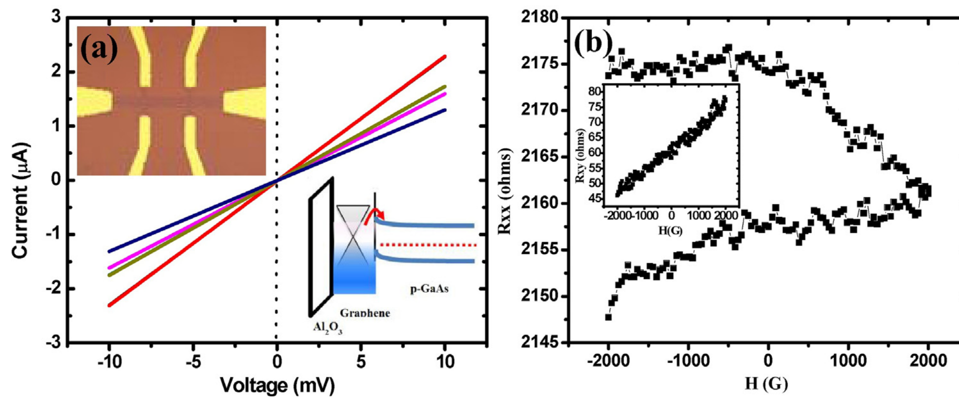

Fig. 4. (a) Electrical characteristics of the graphene layers lying on SiO_2/Si subtracts. Insets are the optical image of Hall-bar device and the schematic illustration of the band energy diagram, respectively (b) Hall resistance of R_{xx} and R_{xy} (inset) at 10 mV range, L = 30 μm and w = 8 μm.

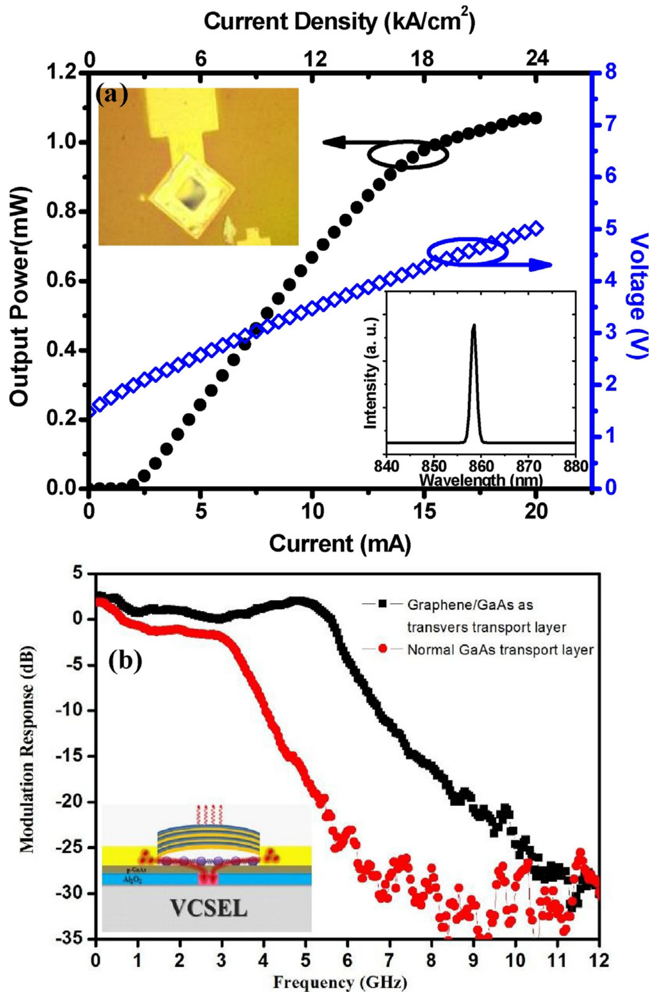

Fig. 5. (a) Light-current-voltage (*L-I-V*) characteristics of VCSEL devices with metal/graphene under cw condition at RT. Insets show the lasing (top left) of VCSELs tested under the probe. The single mode lasing spectrum (bottom right) of the device at a bias of 20 mA is shown as insets. (b) Magnitude of the frequency response of the Gr-VCSEL at 7.5 mA bias current.

insensitive alignment of the two parts without any additional spacing elements, while regulating the waveguide routes with a curved shape guides a strong leaky photons in the lateral direction from the VCSEL into a loss mode, which forms the single transverse mode in the VCSEL with larger oxide aperture. The small signal modulation response of the Gr-VCSEL emitting at 858.5 nm is shown in Fig. 5b for different bias currents. A 3-dB bandwidth of 5.91 GHz is obtained at 4.8 I_{th} comparing to the 3 GHz bandwidth of 3.1 I_{th} bias current for the normal VCSEL. This is because the relatively small modulated bandwidth is probably due to the thermal damping effect that caused by self-heating regime at large bias current. So the dynamic characters of Gr-VCSEL is improved by reducing the lateral resistance through uniform current injection into the laser aperture and thermal limited, leading to enhanced thermal dynamic characteristics and concurrently reduced the series resistance. Moreover, the maximum resonance frequency for the Gr-VCSEL can be carried out by further short the air-gap and reduce oxide-aperture size.

In summary, the single transverse mode VCSELs with top curved dielectric-DBR and top metal/graphene-based electrode are demonstrated here. The technique is described for directly grown dielectric bubble DBR structure on van der Waals Force (vdWF) graphene/half-VCSEL primarily based on the graphene functions not only as the charge transport channel but also as the buffer layer. An average single mode output power of 1.2 mW and threshold current less than 2 mA are achieved for devices with 7 μm oxide apertures. The Gr-VCSEL structure is well optimized for high-speed operation. M Such preliminary results and the potentiality of the modifications into the laser devices motivate us to investigate this approach in the future. This technique could prove to be a viable alternative to conventional and matured 850 nm GaAs-VCSELs.

Acknowledgments

We acknowledge the support of Natural Science Foundation of China under Award#: 60908012 and National Science Foundation of US under Award#: EFRI-1433541, Natural Science Foundation of Beijing under Award#:4143059 and Fondation of Beijing Municipal Education Commission under Grant No. KM201010005030.

References

[1] A. Mutig, D. Bimberg, Adv. Opt. Technol. 2011 (2011) 290508.
[2] S.A. Blokhin, M.A. Bobrov, N.A. Maleev, A.G. Kuzmenkov, A.V. Sakharov, A.A. Blokhin, P. Moser, J.A. Lott, D. Bimberg, V.M. Ustinov, Appl. Phys. Lett. 105 (2014) 061104.
[3] O. Witzel, A. Klein, C. Meffert, S. Wagner, S. Kaiser, C. Schulz, V. Ebert, Opt. Express 21 (2013) 19951.
[4] M. Nakahama, T. Sakaguchi, A. Matsutani, F. Koyama, Appl. Phys. Lett. 105 (2014) 091110.
[5] D.L. Boiko, G. Guerrero, E. Kapon, J. Appl. Phys. 100 (2006) 103102.
[7] A. Moser, E.E. Latta, J. Appl. Phys. 71 (1992) 4848.
[8] K. Iga, IEEE J. Sel. Top. Quantum Electron. 6 (2000) 1201.
[9] D.F. Siriani, K.D. Choquette, IEEE J. Quantum Electron. 47 (2011) 160.
[10] A. Haglund, J.S. Gustavsson, J. Vukusic, P. Modh, A. Larsson, IEEE Photon. Technol. Lett. 2 (2004) 368.
[11] C.M. Long, L. Mutter, B. Dwir, A. Mereuta, A. Caliman, A. Sirbu, V. Iakovlev, E. Kapon, Opt. Express 22 (2014) 21137.

[12] D.S. Song, S.H. Kim, H.G. Park, C.K. Kim, Y.H. Lee, Appl. Phys. Lett. 80 (2002) 3901.
[13] A.K. Geim, Science 324 (2009) 1530.
[14] L. Changgu, W. Xiaoding, J.W. Kysar, J. Hone, Science 321 (2008) 385.
[15] S. Chen, Q.Z. Wu, C. Mishra, J. Kang, H. Zhang, K. Cho, W. Cai, A.A. Balandin, R.S. Ruoff, Nature Mater. 11 (2012) 203–207.
[16] J. Kim, C. Bayram, H. Park, C.W. Cheng, C. Dimitrakopoulos, J.A. Ott, K.B. Reuter, S.W. Bedel, D.K. Sadana, Nat. Commun. 5 (2014) 4836.
[17] Y. Alaskar, S. Arafin, D. Wickramaratne, M.A. Zurbuchen, L. He, J. McKay, Q. Lin, M.S. Goorsky, R.K. Lake, K.L. Wang, Adv. Funct. Mater. 24 (2014) 6629.
[18] B.L. Guan, X.J. Ren, L. Chuan, L. Shuo, G.Z. Shi, X. Guo, Chin. Phys. B 20 (2011) 094206.
[19] X.S. Li, W. Cai, J. An, S. Kim, J. Nah, D. Yang, R. Piner, A. Velamakanni, I. Jung, E. Tutuc, S.K. Banerjee, L. Colombo, R.S. Ruoff, Science 324 (2009) 1312.
[20] P. Yeh, A. Yariv, Chi-Shain Hong, J. Opt. Soc. Am. 67 (1977) 423.
[21] S.P. Koenig, N.G. Boddeti, M.L. Dunn, J. Scott Bunch, Nat. Nanotechnol. 6 (2011) 543.
[22] W. Gao, R. Huang, J. Phys. D: Appl. Phys. 44 (2011) 452001.
[23] N. Moll, A. Kley, E. Pehlke, M. Scheffler, Phys. Rev. B 54 (1996) 8844.
[24] C. Messmer, J.C. Bilello, J. Appl. Phys. 52 (1981) 4623.
[25] J.L. Tedesco, B.L. VanMil, R.L. Myers, J.M. McCrate, S.A. Kitt, P.M. Campbell, G.G. Jernigan, J.C. Culbertson, C.R. Eddy Jr., D.K. Gaskill, Appl. Phys. Lett. 95 (2009) 122102.
[26] O. Zohni, G. Buckner, T. Kim, A. Kingon, J. Maranchi, R. Siergie, J. Micromech. Microeng. 17 (2007) 1042.
[27] P. Temple-Boyer, C. Rossi, E. Saint-Etienne, E. Scheid, J. Vac. Sci. Technol. A 16 (1998) 2003.